Nanoscale

PAPER

View Article Online
View Journal | View Issue

Cite this: *Nanoscale*, 2024, **16**, 10656

A hydrogel-functionalized silver nanocluster for bacterial-infected wound healing†

Zhezhen Wei,[a] Tingting Xu,[a] Cong Wang,[b] Shuai Liu,[a] Wenjing Zhang,[a] Jianan Sun,[a] Huan Yu,*[b] Hui Shi*[a] and Yongbo Song *[a]

Received 2nd April 2024,
Accepted 2nd May 2024

DOI: 10.1039/d4nr01447b

rsc.li/nanoscale

The ever-growing challenges of traditional antibiotic therapy and chronic wound healing have created a hot topic for the development and application of new antimicrobial agents. Silver nanoclusters (Ag NCs) with ultrasmall sizes (<2 nm) and antibacterial effects are promising candidates for next-generation antibiotics, particularly against multi-drug resistant strains. However, the biosafety in the clinical application of Ag NCs remains suboptimal despite some existing studies of Ag NCs for biomedical applications. Considering this, an ultrasmall Ag NC with excellent water solubility was synthesized by a two-phase ligand-exchange method, which exhibits broad-spectrum antibacterial performance. The minimum inhibitory concentrations of Ag NCs against *MRSA*, *S. aureus*, *P. aeruginosa* and *E. coli* were evaluated as 50, 80, 5 and 5 μg mL^{-1}, respectively. Furthermore, a carbomer hydrogel was prepared to be incorporated into the Ag NCs for achieving excellent biocompatibility and biosafety. *In vitro* experiments demonstrate that the Ag NC-gel exhibits good antibacterial properties with lower cytotoxicity. Finally, *in vivo* experiments suggest that this ultrasmall Ag NC functionalized with the hydrogel can serve as an effective and safe antimicrobial agent to aid in wound healing.

[a]*School of Biomedical Engineering, Research and Engineering Center of Biomedical Materials, Anhui Medical University, Hefei, Anhui 230032, China. E-mail: shihui@ahmu.edu.cn, ybsong860@ahmu.edu.cn*
[b]*School of Pharmacy, Anhui Medical University, Hefei 230032, China. E-mail: hyu@ahmu.edu.cn*

†Electronic supplementary information (ESI) available. See DOI: https://doi.org/10.1039/d4nr01447b

Yongbo Song

Dr Yongbo Song obtained his B.S. degree in agriculture from Anhui Agricultural University (2012) and his PhD degree in organic chemistry from Anhui University (2017). He studied at Carnegie Mellon University as a visiting student from 2016 to 2017. He worked at Anhui University as an assistant professor from 2017 to 2020. In 2020, he joined the School of Biomedical Engineering of Anhui Medical University (AHMU). He is now a full professor and his current research focuses on the design of functional metal nanoclusters for biomedical applications.

Introduction

Currently, bacterial infection poses a severe global challenge, presenting a pervasive threat to human health.[1] The excessive use of antibiotics has led to the emergence of drug-resistant superbugs and the absence of effective measures could cause an annual mortality rate of 10 million people by 2050.[2] However, the development of conventional antibiotics is both time-consuming and expensive. Moreover, the rapid evolution of bacterial resistance can significantly undermine their efficacy, ultimately rendering them ineffective.[3,4] The development of novel antibiotics, therefore, represents a promising strategy to ameliorate this grave situation.

In recent years, Ag-based nanomaterials have been widely utilized for the treatment of bio-burns, burns, wounds, and other bacterial infections owing to their non-resistance, low toxicity, and broad-spectrum antibacterial properties.[5–7] Among them, it has been proved that ultrasmall silver nanoclusters (NCs, <2 nm) exhibit excellent antibacterial activity, and their antibacterial performance can be effectively regulated by controlling the types of surface ligands and the composition of metal cores.[8–10] The antibacterial activity of Ag NCs can be ascribed to four primary mechanisms: (1) the generation of reactive oxygen species (ROS) *via* redox reactions,[11–13] (2) the adhesion of Ag NCs to the bacterial cell membrane induces destabilization,[14–16] (3) repression of DNA replication and transcription is observed upon the introduction of Ag NCs

into DNA bases,[17] and (4) Ag^+ ions are released from Ag NCs due to the higher surface to volume ratio.[18–20] It is worth noting that Ag^+ ions can efficiently disrupt the bacterial cell membranes, and the high concentration of Ag^+ ions will induce some side effects on normal mammalian cells such as oxidative stress.[21–23] Therefore, a platform for controlling the release of Ag NCs should be established, which can not only extend the antibacterial duration, but also reduce the concentration of Ag^+ ions.

In the field of nanomedicine, carbomer hydrogels are commonly used as ideal support materials for loading drugs or antibacterial agents to achieve long-lasting bacteriostasis due to their controllable release characteristics.[24–28] In addition, carbomer hydrogels exhibit enhanced moisture retention properties, thereby facilitating the maintenance of a moist wound surface (which is conducive to healing).[29] Some studies have also substantiated the safety profile of carbomers as drug carriers.[30,31] Therefore, the utilization of carbomer hydrogels to incorporate Ag NCs may mitigate the potential cytotoxicity resulting from Ag^+ ions.

In this study, an ultrasmall monodisperse Ag NC (<2 nm)[32–34] was efficiently synthesized using a two-phase ligand-exchange method, which was characterized by polyacrylamide gel electrophoresis (PAGE), UV-vis spectroscopy, transmission electron microscopy (TEM) and X-ray photoelectron spectroscopy (XPS). The *in vitro* antibacterial experiments reveal that this Ag NC possesses exceptional antibacterial activity against both Gram-positive and Gram-negative bacteria. Additionally, a carbomer hydrogel was prepared to be incorporated into the Ag NCs (Ag NC-gel), which not only significantly enhanced their biocompatibility but also provided a stable scaffold for their immobilization. Finally, the effect of Ag NC-gel on infected wound healing was investigated by evaluating the wound closure ratio, collagen deposition and the expression of angiogenesis-related cytokines (CD31). These findings suggest that this Ag NC-gel holds promising potential for application in the treatment of skin damage.

Results and discussion

Characterization of the Ag NCs and Ag NC-gel

The crude product, which shows a broad peak at 480 nm dissolved in water in the UV-vis absorption spectrum (Fig. S1†), was prepared by a two-phase ligand-exchange method at room temperature, in which the varying bond strength between Ag–S and Ag–P was taken into consideration (see the ESI† for details). First, the crude product was analysed by PAGE, in which a prominent brown band is observed with three thin bands (Fig. S2†). The prominent brown band was cut off and extracted with deionized water, and then washed several times with MeOH to obtain the monodisperse Ag NC. The aqueous solution of the as-prepared Ag NC displays two shoulder peaks at 350 and 485 nm (Fig. 1a), which is obviously different from the typical surface plasmon band (460 nm) of large-sized Ag nanoparticles, indicating its molecular state.[35]

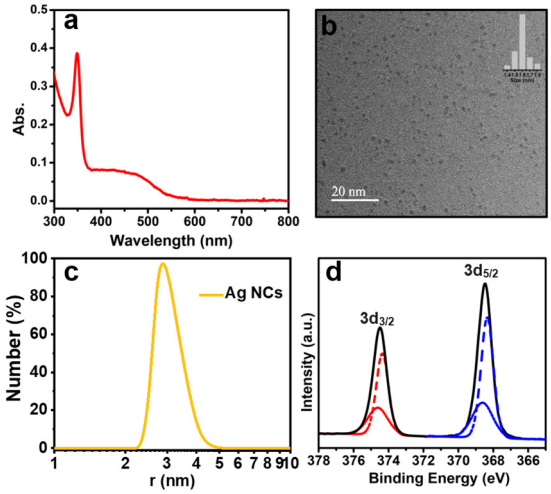

Fig. 1 Characterization of the as-prepared Ag NCs: (a) UV-vis absorption spectrum; (b) TEM image (inset: statistical size distribution); (c) DLS histogram; and (d) XPS spectrum.

Moreover, the TEM image shows that the as-prepared Ag NC possessed an excellent dispersion and uniform size with a diameter of 1.6 nm (Fig. 1b). The hydrodynamic size of this Ag NC was determined by dynamic light scattering (DLS), which is ~2.74 nm (Fig. 1c).

To further analyze the valence state of Ag atoms in the Ag NC, the XPS was performed. As displayed in Fig. 1d, the binding energies of Ag $3d_{3/2}$ Ag $3d_{5/2}$ was determined to be 374.47 and 368.48 eV, respectively. The peaks of Ag $3d_{3/2}$ and Ag $3d_{5/2}$ can be further resolved into two sets of individual peaks (red line: 374.61 and 374.32 eV, blue line: 368.63 and 368.34 eV), which demonstrates the existence of both Ag^0 and Ag^{1+} in this Ag NC,[36,37] suggesting the core–shell structure of the as-prepared Ag NC. In addition, the zeta potential value obtained for the Ag NC was found to be nearly −16.8 ± 2.7 mV (Fig. S3†), which represents the stability of the as-prepared Ag NC.[17] Unfortunately, the acquisition of the electrospray ionization mass spectrum (ESI-MS) for this Ag NC was unsuccessful.

The carbomer hydrogel was prepared based on the previously reported photochemical method,[26] and the Ag NC-gel was obtained by directly dispersing the Ag NCs into the hydrogel through a self-organizing blend. As shown in Fig. S4a,† upon doping Ag NCs into the hydrogel, the Ag NC-gel displays translucent brown color and shows a similar UV-vis absorption spectrum to that of pure Ag NCs. The rheological properties of the gel and Ag NC-gel were then assessed (Fig. S4b†). The Ag NC-gel displayed higher modulus than the blank hydrogel, demonstrating the formation of a stronger hydrogel. This phenomenon can be ascribed to the additional H-bonding induced by the carboxylic or amino groups from the surface protecting ligands in the Ag NCs, which will control the release rate of Ag NCs. Moreover, if the Ag NC-gel (100 μg mL^{-1}) was soaked in deionized water for 4 h, only some light brown solution can be obtained after centrifugation (Fig. S5†),

which also exhibits the same optical properties as pure Ag NCs and does not produce any white precipitate upon adding 2 mg of NaCl. These results indicate the good stability and slow-release of Ag NCs in the Ag NC-gel. The micro structure of the Ag NC-gel was assessed using scanning electron microscopy (SEM), which shows a smooth, loose, and porous structure surface (Fig. S6a†). Furthermore, the uniform distribution of Ag NCs in the hydrogels was also testified by elemental mapping (Fig. S6b†).

Evaluation of antibacterial activity *in vitro*

The antibacterial effect of the free Ag NCs was evaluated using Gram-positive bacteria (*MRSA* and *S. aureus*) and Gram-negative bacteria (*P. aeruginosa* and *E. coli*) models. Generally, a series of comparative tests were conducted to determine the most appropriate conditions of antibacterial ability. The Ag NCs were co-cultured with the four strains in a 96-well plate at different concentrations. After overnight incubation, the concentration of Ag NCs, which keep the bacterial liquid transparent, was considered as the minimum inhibitory concentration (MIC). According to this method, the MIC values of Ag NCs against *MRSA*, *S. aureus*, *P. aeruginosa*, and *E. coli* were determined as 50 μg mL^{-1}, 80 μg mL^{-1}, 5 μg mL^{-1}, and 5 μg mL^{-1}, respectively (Fig. S7†).

To further elucidate the optimal antibacterial concentration of Ag NCs, the agar plate counting method was employed. Starting from the MIC concentration, 100 μL of bacterial suspension was aspirated from the 96-well plate using a pipette, and then evenly spread on an agar plate using a spreader. The minimum bactericidal concentration (MBC) of Ag NCs against *MRSA*, *S. aureus*, *P. aeruginosa*, and *E. coli* were determined to be 100 μg mL^{-1}, 120 μg mL^{-1}, 20 μg mL^{-1}, and 20 μg mL^{-1}, respectively (Fig. S8†), in which no bacterial colonies were observed. These results show that this Ag NC exhibits superior bactericidal efficacy against Gram-negative bacteria in comparison with Gram-positive bacteria, which is similar to other studies.[38–40] This phenomenon may be attributed to the fact that the peptidoglycan layer in the cell walls of Gram-positive bacteria is 30 nm thick, whereas it is only 2–3 nm thick in Gram-negative bacteria.[41] The thicker peptidoglycan layer may serve as a protective barrier to impede the penetration of Ag NCs into the cytoplasm and thereby ensuring the comparatively lower sensitivity of Gram-positive bacteria in comparison with their Gram-negative counterparts.[42]

In addition, the antibacterial efficiency of Ag NCs was quantified by the colony forming units (CFU). With increasing concentrations of Ag NCs, there was a significant reduction in the bacterial count (Fig. 2a and b). For *E. coli*, the bacterial survival rates were 84.27%, and 23.42% when the concentration of Ag NCs was at 1/4 MBC and 1/2 MBC, respectively. In the case of *MRSA*, the bacterial survival rate decreased from 60.71% to 14.39% with the concentration ranging from 1/4 MBC to 1/2 MBC. Similarly, the survival rate of *P. aeruginosa* and *S. aureus* at concentrations of 0, 1/4 MBC, 1/2 MBC, and the MBC were studied, in which the antibacterial efficiency is positively correlated with the concentration of Ag NCs (Fig. S9†). Furthermore, the bacterial growth curve was measured to explore the effect of Ag NCs on bacterial growth kinetics. The optical density (OD) at 600 nm was measured as the number density value of bacterial cells. The growth trend showed a sigmoidal increase at the concentration of 1/4 MBC for both *E. coli* and *MRSA*, in which the maximum values are lower than those in the absence of Ag NCs. These findings suggest that the Ag NCs can inhibit the bacterial growth and reproduction. As the concentration reaching the bacterial MBC, no bacterial growth was observed (Fig. 2c). This phenomenon was also observed in experiments involving co-incubation of *S. aureus* and *P. aeruginosa* (Fig. S10†).

Subsequently, the fluorescence staining method was employed to further validate the antibacterial effect of Ag NCs using *MRSA* and *E. coli* as models. The inverted fluorescence microscopy images in Fig. 2d–f demonstrate that co-incubation of bacteria with varying concentrations of Ag NCs leads to a significant increase in red fluorescence intensity originating from the damaged bacteria. At the MBC of Ag NCs, an elevated level of red fluorescence is observed without any concurrent green fluorescence, indicating complete bacterial inactivation. These findings highlight the exceptional antibacterial properties of the as-prepared Ag NCs.

Cell toxicity and antibacterial activity of Ag NC-gel

Hydrogels are currently considered as ideal candidate materials for wound dressing due to their high water permeability, controlled drug release, and biocompatible properties.[43,44] Thus, the cellular MTT assay was performed to evaluate the survival rate of cells incubated with the Ag NCs and Ag NC-gel for 24 hours, respectively. As can be seen from Fig. S11,† the toxicity of Ag NCs was observed to increase with increasing concentration, leading to a decrease in cell viability to 56.93% at a concentration of 150 μg mL^{-1}. However, the MTT results of Ag NC-gel illustrate that even at the same concentration of 150 μg mL^{-1}, the cell viability remained high at 96.94%. This discrepancy can be attributed to its slow release of Ag NCs.

To evaluate the antibacterial efficacy of Ag NC-gel, the agar diffusion method was employed to measure the size of the inhibition zone. Herein, *E. coli* densities of 10^7 and 10^5 were selected for bacteriostasis experiments, while the concentrations of Ag NCs in the hydrogel were 0, 60, 80, and 100 μg mL^{-1}, respectively. For *MRSA*, the bacterial density was increased to 10^9 and 10^7 and the concentration of Ag NCs ranged from 0 to 150 μg mL^{-1} (Fig. 3a). As shown in Fig. 3b, the pure hydrogel group exhibited no inhibition zone against the tested bacteria. In contrast, the composite materials showed a gradual increase in the size of the inhibition zone with higher concentrations of Ag NCs. At the maximum concentrations of Ag NCs, the diameter of inhibition zone was found to be 8.9 and 12.6 mm against *E. coli* (10^5 CFU) and *MRAS* (10^7 CFU), respectively. These results suggest that the Ag NC-gel could gradually release the Ag NCs to effectively kill bacteria while maintaining good biocompatibility, indicating

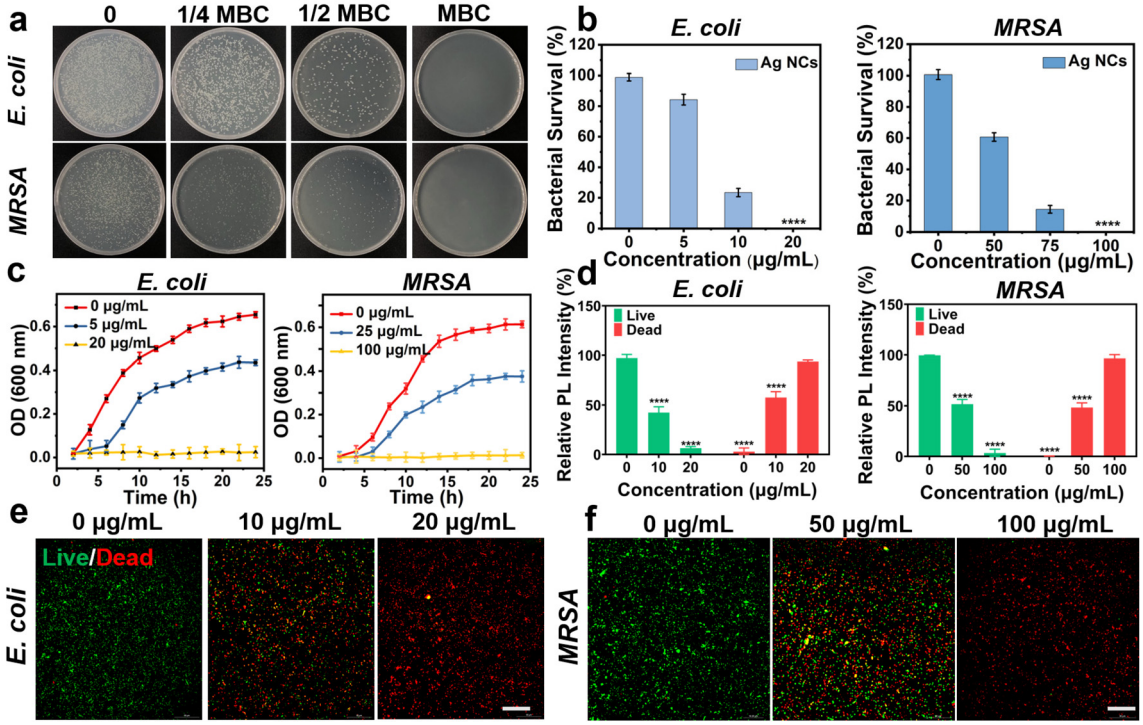

Fig. 2 *In vitro* antibacterial activity of the Ag NCs. (a) Photographs of bacteria colonized by *E. coli* and *MRSA* with different treatments, where *E. coli* were exposed to Ag NCs at 0, 5 (1/4 MBC), 10 (1/2 MBC), and 20 μg mL^{-1} and *MRSA* were exposed to Ag NCs at 0, 25 (1/4 MBC), 50 (1/2 MBC), and 100 μg mL^{-1}. (b) The number of bacterial colonies formed by *E. coli* and *MRSA*. The values are shown as the mean ± SD (n = 3). (c) Cell growth curves recorded over time starting from an OD600 value at 0.1, where *E. coli* and *MRSA* were exposed to the Ag NCs at different concentrations. (d–f) Fluorescence staining images of *E. coli* and *MRSA* bacteria using SYTO9/PI after different treatments and the corresponding relative fluorescence. Scale bar is 50 μm. Statistical analysis was performed using the two-tailed Student's t-test (****p < 0.0001, ***p < 0.001, **p < 0.01, and *p < 0.05).

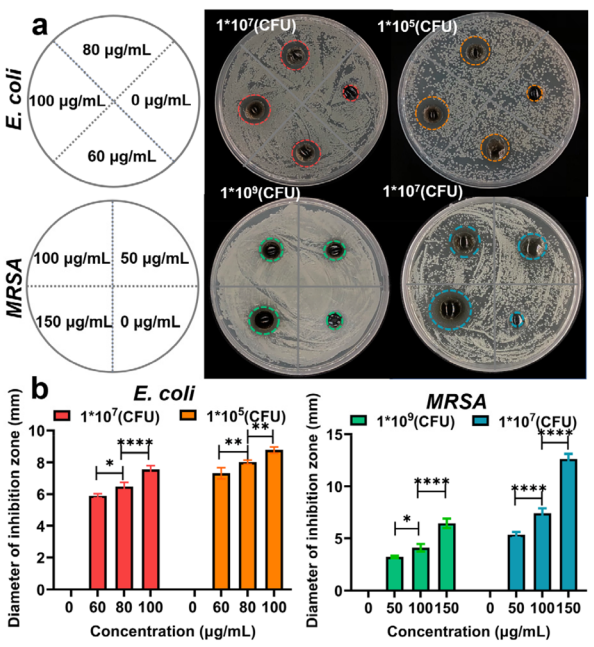

Fig. 3 Evaluation of the antibacterial activity of Ag NC-gel. (a) Photographs of antibacterial activity against *E. coli* and *MRSA*. (b) Statistics of the inhibitory zone diameter (****p < 0.0001, ***p < 0.001, **p < 0.01, and *p < 0.05).

its potential for future applications in bacterial-infected wound healing.

In vivo wound healing efficiency of Ag NC-gel

To evaluate the *in vivo* effects of the Ag NC-gel on wound healing, an mouse bacterial wound infection model was established (Fig. 4a). After creating the wounds (10 mm) in the mice, the pre-prepared *MRSA* suspension was dropped onto the wound surface, and a 4-hour infection period was allowed. Subsequently, the Ag NC-gel (150 μg mL^{-1}) was sprayed on the *MRSA*-infected wound. The *in vivo* wound healing efficiency of PBS (as the control group), the gel and the Ag NC-gel was explored by creating wounds in the mice. As shown in Fig. 4b, the photographs of wound healing in each group were obtained on days of 0, 2, 4, 6 and 8, and the corresponding wound areas were also counted. These results illustrate that the Ag NC-gel group exhibits significantly higher efficiency in wound healing compared to the other groups. As can be seen from the histogram of the wound closure rate (Fig. 4c), the average wound closure rate on day 4 of Ag NC-gel was determined to be 55.46%, which is better than those of PBS (21.73%) and the gel (17.96%). On the 8th day, the wounds of the Ag NC-gel group were almost completely healed with an average wound closure rate of 94.44%; however, the wound

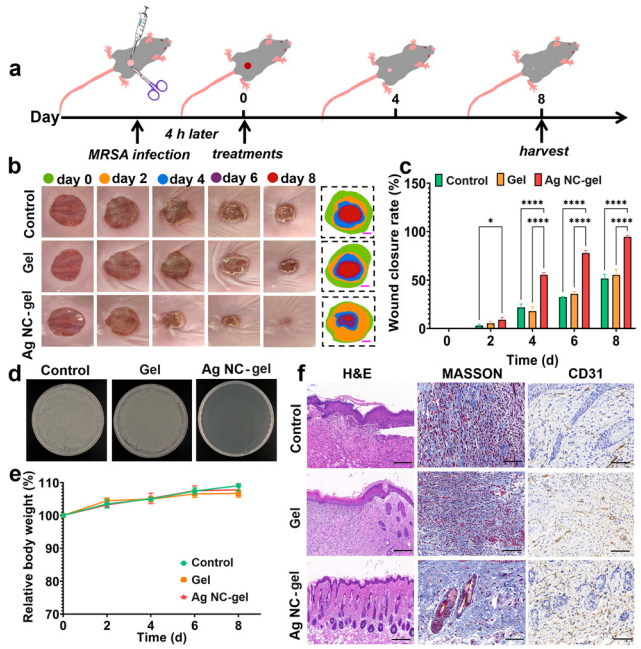

Fig. 4 Effect of the Ag NC-gel on the healing of *MRSA*-infected wounds. (a) Scheme of the *MRSA*-infected wound model and treatments. (b) Infected wound photos in each group and the corresponding wound area traces. Scale bar is 2.5 mm. (c) Wound area statistics in each group. (d) Photos of bacterial colonies of *MRSA*-infected wound tissues at the 8th day. (e) Body weight profile. (f) H&E staining, Masson's trichrome staining and CD31 staining of wound tissues from each group with the corresponding scale bars of 200, 100, and 100 μm. (****p < 0.0001, ***p < 0.001, **p < 0.01, and *p < 0.05).

closure rates of PBS and the gel merely reach to 51.62 and 55.31%, respectively.

To assess the bactericidal effects with the various treatments, the wound tissues of each group on day 8 were collected and an ager-plate counting assay was performed to assess the *MRSA* count. As shown in Fig. 4d, no obvious *MRSA* colonies were observed only in the Ag NC-gel group, which is consistent with the results of wound closure of the Ag NC-gel group. Additionally, the body weights of the mice in each group on days 0, 2, 4, 6 and 8 were also recorded (Fig. 4e), and no notable weight changes in each group were observed. This suggests that the Ag NC-gel has no remarkable toxic effect on the mice. To further evaluate the efficacy of Ag NC-gel in facilitating wound healing, histological analysis was performed on mouse wound tissue using H&E staining on the 8th day. It was observed that the control group exhibited a significant infiltration of neutrophils, and there was thickening of the epidermal layers, indicating the persistent presence of inflammatory factors caused by bacterial infection (Fig. 4f). The wound treated with the Ag NC-gel displayed an increased number of new hair follicles. Similarly, based on Masson's staining results, it could be noted that collagen regeneration in the Ag NC-gel group was higher compared to the other two groups. It worth noting that appropriate deposition and remodelling of collagen are advantageous for enhancing tissue tensile strength, expediting wound tissue reconstruction and promoting healing. Typically, neovascularization facilitates oxygen and nutrient transport to the wound site, supporting fibroblast proliferation, collagen synthesis, and epithelialization. Moreover, CD31 is an important indicator of neovascularization. As depicted in Fig. 4f, there are significantly more angiogenesis observed in the Ag NC-gel group compared to the control and the gel groups. Moreover, the wound healing efficiency of Ag NC-gel (100 μg mL^{-1}) on the *E. coli*-infected wound was also investigated (Fig. S12†), which also illustrates that this Ag NC-gel possesses significantly higher efficiency in *E. coli*-infected wound healing.

In vivo biological safety investigation

Herein, the *in vivo* toxicity was ultimately assessed to clarify the safety profile of Ag NC-gel, in which blood biochemical parameters were evaluated on 8th day for each group of mice. As shown in Fig. 5a, the serum levels of liver function indicators (AST/GOT, GPT, Y-GT and AKP) and kidney function (CRE and BUN) in the Ag NC-gel group were monitored, which exhibit no obvious change compared to those in the control and gel groups. This phenomenon demonstrates that the Ag NC-gel has no systemic toxicity. In addition, H&E staining analysis was performed on the major organs (heart, liver, spleen, lungs, and kidneys) of the mice in each group on the 8th day. As displayed in Fig. 5b, the staining results validate that, following treatment with the Ag NC-gel, the tissue structures remained intact without significant indications of inflammatory damage or organ injury. Finally, the residual silver

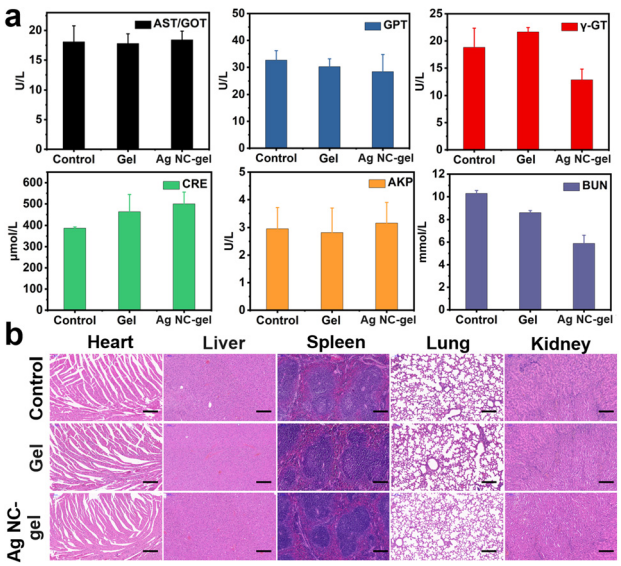

Fig. 5 (a) Serum levels of liver function indicators: aspartate transaminase (AST/GOT), alanine transaminase (GPT), γ-glutamyl transferase enzyme (γ-GT) and alkaline phosphatase (AKP); serum levels of kidney function indicators: creatinine (CRE) and blood urea nitrogen (BUN); blood parameters of mice with different treatments for 8 days. (b) H&E staining images of the major organs (heart, liver, spleen, lung, and kidney) from the mice after 8 days of treatment with the control, gel, and Ag NC-gel, respectively. Scale bar is 100 μm.

element in the major internal organs (heart, liver, spleen, lungs, and kidneys) were detected by ICP-MS (Fig. S13†), in which very trace amounts of silver element were observed (<0.1 μg). In generally, all these results strongly demonstrate the efficacy and safety of Ag NC-gel as a platform for treating bacterial infection and promoting wound healing.

Conclusions

In summary, a water-soluble Ag NC with ultrasmall size was prepared *via* a two-phase ligand-exchange method, which exhibits significant antibacterial ability against both Gram-positive and Gram-negative bacteria. Moreover, a carbomer hydrogel was developed to functionalize the Ag NC, effectively preserving its excellent antibacterial efficacy while significantly enhancing its cytotoxicity, thus yielding an ideal wound dressing. *In vivo* experiments on infected wound healing demonstrate that this Ag NC-gel could remarkably accelerate the rate of wound closure through its exceptional bactericidal activity and anti-inflammatory performance. More importantly, this Ag NC-gel also exhibits excellent biosafety, rendering it highly promising as an antimicrobial agent for facilitating the healing of infected wounds.

Ethics statement

The Balb/c female mice (8 weeks) were obtained from the Laboratory Animal Center at Anhui Medical University (Hefei, Anhui Province, China), and all the animal experiments were conducted following the guidance and approval of the Ethical Committee of Anhui Medical University (approval number: LLSC20231653). All animal experimental procedures were performed in accordance with the Regulations for the Administration of Affairs Concerning Experimental Animals approved by the State Council of People's Republic of China.

Conflicts of interest

There are no conflicts to declare.

Acknowledgements

This work was financially supported by the Natural Science Foundation of China (Grant No. 22171007, 12004008 and 21801001), the Natural Science Key Project from the Department of Education of Anhui Province (Grant No. KJ2021A0250) and the Scientific Research of BSKY (Grant No. XJ2020026) from Anhui Medical University. The authors thank the Center for Scientific Research of Biomedical Engineering, Anhui Medical University for providing valuable help in our experiments.

References

1 X. He, Y. Yang, Y. Guo, S. Lu, Y. Du, J.-J. Li, X. Zhang, N. L. C. Leung, Z. Zhao, G. Niu, S. Yang, Z. Weng, R. T. K. Kwok, J. W. Y. Lam, G. Xie and B. Z. Tang, *J. Am. Chem. Soc.*, 2020, **142**, 3959–3969.
2 C. Willyard, *Nature*, 2017, **543**, 15–15.
3 A. J. Huh and Y. J. Kwon, *J. Controlled Release*, 2011, **156**, 128–145.
4 K. Y. Zheng, M. I. Setyawati, D. T. Leong and J. P. Xie, *Coord. Chem. Rev.*, 2018, **357**, 1–17.
5 X. Mao, R. Cheng, H. Zhang, J. Bae, L. Cheng, L. Zhang, L. Deng, W. Cui, Y. Zhang, H. A. Santos and X. Sun, *Coord. Chem. Rev.*, 2019, **6**, 1801555.
6 P. Dutta and B. Wang, *Coord. Chem. Rev.*, 2019, **383**, 1–29.
7 S. Tang and J. Zheng, *Adv. Healthcare Mater.*, 2018, **7**, 1701503.
8 Z. Wang, Y. Fang, X. Zhou, Z. Li, H. Zhu, F. Du, X. Yuan, Q. Yao and J. Xie, *Nano Res.*, 2020, **13**, 203–208.
9 X. Yuan, M. I. Setyawati, D. T. Leong and J. P. Xie, *Nano Res.*, 2014, **7**, 301–307.
10 K. Y. Zheng, M. I. Setyawati, T. P. Lim, D. T. Leong and J. P. Xie, *ACS Nano*, 2016, **10**, 7934–7942.
11 Y. J. Chen, L. T. Ren, L. X. Sun, X. Bai, G. Q. Zhuang, B. Cao, G. Q. Hu, N. F. Zheng and S. J. Liu, *NPG Asia Mater.*, 2020, **12**, 56.
12 S. Javani, R. Lorca, A. Latorre, C. Flors, A. L. Cortajarena and A. Somoza, *ACS Appl. Mater. Interfaces*, 2016, **8**, 10147–10154.
13 X. Yuan, M. I. Setyawati, A. S. Tan, C. N. Ong, D. T. Leong and J. P. Xie, *NPG Asia Mater.*, 2013, **5**, e39.
14 X. T. Yan, B. He, L. H. Liu, G. B. Qu, J. B. Shi, L. Hu and G. B. Jiang, *Metallomics*, 2018, **10**, 557–564.
15 S. U. Khan, T. A. Saleh, A. Wahab, M. H. U. Khan, D. Khan, W. U. Khan, A. Rahim, S. Kamal, F. U. Khan and S. Fahad, *Int. J. Nanomed.*, 2018, **13**, 733–762.
16 R. E. Duval, J. Gouyau and E. Lamouroux, *Nanomaterials*, 2019, **9**, 1775.
17 J. C. Jin, X. J. Wu, J. Xu, B. B. Wang, F. L. Jiang and Y. Liu, *Biomater. Sci.*, 2017, **5**, 247–257.
18 Y. Zheng, M. Wei, H. Wu, F. Li and D. Liang, *J. Nanobiotechnol.*, 2022, **20**, 328.
19 F. Wang, M. Sun, D. Li, X. Qin, Y. Liao, X. Liu, S. Jia, Y. Xie and C. Zhong, *Small*, 2023, 2303591.
20 R. Tumskiy, B. Khlebtsov, A. Tumskaia, S. Evstigneeva, E. Antoshkina, A. Zakharevich and N. G. Khlebtsov, *Int. J. Mol. Sci.*, 2023, **24**, 8306.
21 X. L. Xie, T. C. Sun, J. Z. Xue, Z. H. Miao, X. Yan, W. W. Fang, Q. Li, R. P. Tang, Y. Lu, L. X. Tang, Z. B. Zha and T. He, *Adv. Funct. Mater.*, 2020, **30**, 2000511.
22 P. V. AshaRani, G. L. K. Mun, M. P. Hande and S. Valiyaveettil, *ACS Nano*, 2009, **3**, 279–290.
23 F. Carrouel, S. Viennot, L. Ottolenghi, C. Gaillard and D. Bourgeois, *Nanomaterials*, 2020, **10**, 140.
24 C. Y. Chen, H. Yin, X. Chen, T. H. Chen, H. M. Liu, S. S. Rao, Y. J. Tan, Y. X. Qian, Y. W. Liu, X. K. Hu,

M. J. Luo, Z. X. Wang, Z. Z. Liu, J. Cao, Z. H. He, B. Wu, T. Yue, Y. Y. Wang, K. Xia, Z. W. Luo, Y. Wang, W. Y. Situ, W. E. Liu, S. Y. Tang and H. Xie, *Sci. Adv.*, 2020, **6**, eaba0942.

25 Z. S. Ruan, C. L. Zhang, T. W. Shi, Z. Y. Luo, Y. A. Zhang, Z. X. Cao, R. T. Huang, Y. F. Chen and D. X. Cui, *Mater. Today Bio*, 2022, **16**, 100426.

26 B. A. Khan, A. Ali, K. M. Hosny, A. A. Halwani, A. M. Almehmady, M. Iqbal, W. S. Alharbi, W. A. Abualsunun, R. B. Bakhaidar, S. S. A. Murshid and M. K. Khan, *Drug Delivery*, 2022, **29**, 52–61.

27 Q. Hui, L. Zhang, X. Yang, B. Yu, Z. Huang, S. Pang, Q. Zhou, R. Yang, W. Li, L. Hu, X. Li, G. Cao and X. Wang, *ACS Biomater. Sci. Eng.*, 2018, **4**, 1661–1668.

28 R. I. Mustafin, T. V. Kabanova, I. I. Semina, A. V. Bukhovets, V. R. Garipova, E. V. Shilovskaya, S. F. Nasibullin, A. Y. Sitenkov, R. R. Kazakova and V. A. Kemenova, *Pharm. Chem. J.*, 2011, **45**, 491–494.

29 Y. Huang, F. Shi, L. Wang, Y. Yang, B. M. Khan, K. L. Cheong and Y. Liu, *Int. J. Biol. Macromol.*, 2019, **132**, 729–737.

30 M. Luo, Q. Shen and J. Chen, *Int. J. Nanomed.*, 2011, **6**, 1603–1610.

31 C. Debbasch, S. B. De La Salle, F. Brignole, P. Rat, J.-M. Warnet and C. Baudouin, *Invest. Ophthalmol. Visual Sci.*, 2002, **43**, 3409–3415.

32 R. Jin, C. Zeng, M. Zhou and Y. Chen, *Chem. Rev.*, 2016, **116**, 10346–10413.

33 K. Y. Zheng and J. P. Xie, *Trends Chem.*, 2020, **2**, 665–679.

34 J.-C. Jin, X.-J. Wu, J. Xu, B.-B. Wang, F.-L. Jiang and Y. Liu, *Biomater. Sci.*, 2017, **5**, 247–257.

35 H. Yang, Y. Wang, X. Chen, X. Zhao, L. Gu, H. Huang, J. Yan, C. Xu, G. Li, J. Wu, A. J. Edwards, B. Dittrich, Z. Tang, D. Wang, L. Lehtovaara, H. Häkkinen and N. Zheng, *Nat. Commun.*, 2016, **7**, 12809.

36 H. Li, Y. Song, Y. Lv, Y. Yun, X. Lv, H. Yu and M. Zhu, *Inorg. Chem.*, 2019, **58**, 1724–1727.

37 H. Haidari, R. Bright, Z. Kopecki, P. S. Zilm, S. Garg, A. J. Cowin, K. Vasilev and N. Goswami, *ACS Appl. Mater. Interfaces*, 2022, **14**, 390–403.

38 J. Gouyau, R. E. Duval, A. Boudier and E. Lamouroux, *Int. J. Mol. Sci.*, 2021, **22**, 1905.

39 J. S. Kim, E. Kuk, K. N. Yu, J. H. Kim, S. J. Park, H. J. Lee, S. H. Kim, Y. K. Park, Y. H. Park, C. Y. Hwang, Y. K. Kim, Y. S. Lee, D. H. Jeong and M. H. Cho, *Nanomedicine*, 2007, **3**, 95–101.

40 C. Quintero-Quiroz, N. Acevedo, J. Zapata-Giraldo, L. E. Botero, J. Quintero, D. Zárate-Triviño, J. Saldarriaga and V. Z. Pérez, *Biomater. Res.*, 2019, **23**, 27.

41 T. T. Hanh, N. T. Thu, N. Q. Hien, P. N. An, T. T. K. Loan and P. T. Hoa, *Radiat. Phys. Chem.*, 2016, **121**, 87–92.

42 A. L. Kubo, I. Capjak, I. V. Vrcek, O. M. Bondarenko, I. Kurvet, H. Vija, A. Ivask, K. Kasemets and A. Kahru, *Colloids Surf., B*, 2018, **170**, 401–410.

43 Q. Bai, K. Han, K. Dong, C. Zheng, Y. Zhang, Q. Long and T. Lu, *Int. J. Nanomed.*, 2020, **15**, 9717–9743.

44 Y. S. Zhang and A. Khademhosseini, *Science*, 2017, **356**, 500.